DOI: 10.1002/cphc.200900283

A Comparative Study of the Structural, Electronic, and Vibrational Properties of NH_3BH_3 and $LiNH_2BH_3$: Theory and Experiment

Seung Mi Lee,*[a] Xiang-Dong Kang,[b] Ping Wang,[b] Hui-Ming Cheng,[b] and Young Hee Lee[c]

Herein, we systematically investigate the structural, electronic, and vibrational properties of ammonia borane (NH_3BH_3, AB) and lithium amidoborane ($LiNH_2BH_3$, LAB) through both density functional calculations and experiments. AB and LAB samples are generated and their vibrational spectra are obtained by using Fourier transformed infrared spectroscopy (FTIR). The measured vibrational spectra are in good agreement with the calculated ones. Our calculations show that the Li-related vibration modes are primarily found in the low-frequency region ($<1000\ cm^{-1}$), and that the intermolecular interactions significantly influence the vibrational spectra. Electronic structure calculations provide insights into the differences between the binding natures of AB and LAB and their influence on the vibrational properties of these compounds.

1. Introduction

The use of hydrogen as a clean energy source is highly demanding because of the limited amount of combustive fossil fuels and their environmentally toxic byproducts. High-volume hydrogen gas storage containers are under debate for practical applications. Solid organic/inorganic materials have been used to increase the storage capacity in both weight and volume through condensation to liquid. The main difficulty of hydrogen gas adsorption on these materials arises from the weak interactions between the hydrogen molecules and the surface. Thus, the design rule for these materials is: 1) to incorporate reasonable binding sites so that uptake and release of hydrogen molecules can be conducted near ambient conditions, 2) to increase the effective surface area or micropores and mesopores, and 3) to achieve structural and chemical stability with long-term cycles of hydrogen uptake and release. Up to now, several materials have been investigated but have failed to match all these criteria.

Metal hydrides are traditional candidates for hydrogen storage—because of their highly reversible storage and release processes—but their storage capacity is low, up to only 1–2 wt%.[1] In addition, some metal hydrides (e.g. lithium aluminum hydride) react violently upon exposure to air and are toxic when in contact with the skin, thus hindering their practical applications. Carbon nanotubes (CNT) have been extensively investigated, experimentally and theoretically, as storage candidates.[2–14] In spite of the high surface area of CNTs, the adsorption energy is presumably low so that low temperatures and high pressures are required for hydrogen storage. Inserting hydrogen molecules into the tube through both ends by capillary effects leads to a rather small reaction area due to the high aspect ratio of the nanotube. Modifying the chemical properties by introducing dopants is expected to increase the hydrogen-storage capacity, and several experimental results outreach the 2010 Department of Energy (DOE) target of 6 wt%.[15,16] However, the reported values vary very widely from 0.1[11] to 20 wt%.[3] It is generally believed that moisture plays a dominant role in misinterpreting the precise storage capacity.[13,14] From careful experiments under moisture-free circumstances, the storage capacity from nanotubes is reported as low as only 0.1 wt%, under 1 atm and room temperature.[11] An even smaller value, of 0.005 wt%, has been reported as well.[10] From various experimental and theoretical studies, as briefly summarized above, it is believed that nanotubes themselves are not promising candidates for hydrogen storage.[17,18] Metal-decorated polymers[19] or light-element-doped fullerene[20] are also suggested as promising materials for hydrogen storage, but the theoretically predicted highest hydrogen-storage capacity has not yet been realized in the experiments. Porous materials are also strong candidates due to their relatively light weight and large surface area. Specifically designed metal organic frameworks are reported to store hydrogen molecules up to 7.5 wt%,[21] and covalent organic frameworks have an even higher value of 18.9 wt% at 77 K, but still far below the DOE target at room temperature.[22]

Ammonia borane (NH_3BH_3, AB) has been spotlighted due to its amazingly high storage capacity (of 19.6 wt%) and favora-

[a] Dr. S. M. Lee
Center for Materials Measurements
Korea Research Institute of Standards and Science
Daejeon 305-340 (Republic of Korea)
Fax: (+82) 42-868-5032
E-mail: seungmi.lee@kriss.re.kr

[b] Dr. X.-D. Kang, Dr. P. Wang, Prof. H.-M. Cheng
Shenyang National Laboratory for Materials Science
Institute of Metal Research, Chinese Academy of Sciences
Shenyang 110016 (People's Republic of China)

[c] Prof. Y. H. Lee
Department of Physics, Department of Energy Science
Center for Nanotubes and Nanostructured Composites
Sungkyunkwan Advanced Institute of Nanotechnology
Sungkyunkwan University, Suwon 440-746 (Republic of Korea)

ble thermal stability. However, its slow decomposition speed at moderate temperatures (< 100 °C) and the formation of volatile toxic by-products, such as borazine, hinders the practical application of this compound as a hydrogen-storage material.[23,24] Finding a reversible recharging path from NHBH to NH_3BH_3 is also a huddle to overcome.[25] Recently, lithium amidoborane ($LiNH_2BH_3$, LAB), synthesized by mechanical ball-milling of an AB/LiH mixture, was reported to be air-stable and capable of rapidly releasing more than 7 wt% of pure hydrogen at 100 °C.[26] Although the Li dopant changed the reaction speed and temperature, the origin of the difference in hydrogen decomposition in AB and LAB has not yet been clarified. Understanding the physical and chemical properties of AB and LAB at the atomic level is a pre-requisite for the engineering of hydrogen decomposition. Structural data on AB[27,28] and LAB are amazingly rare, and theoretical calculations on LAB are reported only very recently.[29,30] To date, no vibrational-mode assignment or comprehensive comparison between AB and LAB structures have been reported.

Herein, we systematically investigate AB and LAB materials—from the single-molecule to the bulk-crystal levels—by means of density functional theory (DFT) calculations. The calculated structural properties are in excellent agreement with experimental data. The electronic properties of molecular and crystal forms of AB and LAB are studied by atomic charge analysis, Fukui function, and band-gap calculations. The vibrational properties are also studied by DFT calculations combined with experimental Fourier transform infrared (FTIR) spectroscopy measurements. From the DFT calculations, we found that the vibration of a single molecule was very different from that of the bulk crystal, due to intermolecular interactions. The origins of the FTIR peaks were identified by our DFT calculations. Our study enhances the understanding of the physical properties of AB and LAB materials, which could be used for further applications within the devices.

2. Results and Discussion

2.1. Structural Properties

Figure 1 shows the FTIR spectra of AB and LAB samples. The spectrum of AB is simpler than that of LAB, which can be ascribed to the breaking of degeneracy into splitting by the presence of lithium atoms instead of hydrogen atoms. We can divide the spectra in three regions: region I (below 1600 cm^{-1}), region II (2000–2500 cm^{-1}), and region III (above 3000 cm^{-1}). In region I, the spectrum of LAB is spiky with more abundant peaks than that of AB. In region II, both spectra are roughly similar, but the peaks in the spectrum of LAB are somewhat broader. In the high-frequency region III, broader and more abundant peaks are found in the LAB spectrum. One can assume that the high-frequency peaks originate from bond stretching whereas the peaks in low-frequency region are related to the hydrogen bending modes. Moreover, in the LAB spectrum, the lithium-related peaks are intermixed with hydrogen-related ones, thus leading to ambiguities in the identification of such modes. Therefore, the identification of vibrational modes of each peak required a quantum mechanical level of accurate calculations.

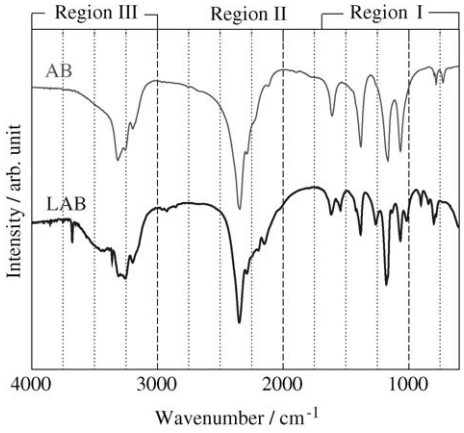

Figure 1. FTIR spectra of AB and LAB crystals. Detailed descriptions of regions I (< 1600 cm^{-1}), II (2000–2500 cm^{-1}), and III (> 3000 cm^{-1}) are given in the text.

Firstly, to understand the structural properties of AB and LAB, their single-molecule structural properties were calculated. The calculated values of the bond length, bond angle, and bond strengths of AB and LAB molecules are listed in Table 1 with experimental data from the CRC handbook.[31] Tto confirm the validity of our calculations, other relevant small molecules, such as H_2, Li_2, LiH, NH_3, NLi_3, BH_3, BLi_3, and B_2H_6, were also calculated and listed together. Experimentally, the BH_3 molecule was highly reactive and easily oxidized, so that only a dimerized form as B_2H_6 (with D_{2h} symmetry) was found in the gaseous state. Note that the NH_3 molecule has C_{3v} point group

Table 1. Bond lengths, bond angles, and bond strengths of several molecules obtained by DFT–LDA calculations.[a,b]

Molecule (*sym.*[c])		Bond length [Å] DFT	Expt.[31]	Bond angle [°] DFT	Expt.[31]	Bond strength [eV] DFT	Expt.[31]
$H_2(D_{\infty h})$		0.764	0.7414	–	–	6.853	4.518
$Li_2(D_{\infty h})$		2.681	2.6729	–	–	0.735	–
$LiH(C_{4v})$		1.610	1.5949	–	–	2.664	2.4671
$NH_3(C_{3v})$		1.024	1.012	105.8	106.7	6.672	4.6917 ± 0.01
$NLi_3(D_{3h})$		1.707	–	120.0	–	3.492	-
$BH_3(D_{3h})$		1.204	–	120.0	–	5.142	-
$BLi_3(D_{3h})$		2.069	–	120.0	–	1.486	-
$B_2H_6(D_{2h})$	H-B	1.201	1.19	97.5	97	5.391	–
		1.313	1.33	108.3	122		
	B···B	1.736	1.77	–	–	7.267	–
$AB(C_{3v})$	H-N	1.024	–	107.9	–	5.800	–
				110.9			
	H-B	1.218	–	105.8	–	5.131	–
	B-N	1.644	–	–	–	2.534	–
$LAB(C_3)$	H-N	1.023	–	112.0	–	5.973	–
	H-B	1.287	–	104.6	–	4.733	–
		1.222		112.3			
	B-N	1.571	–	–	–	4.532	–
	Li-N	1.845	–	77.2	–	3.854	–
				122.6			

[a] The "–" sign indicates that no relevant data are available. [b] AB and LAB are NH_3BH_3 and $LiNH_2BH_3$, respectively. [c] Molecular symmetry.

symmetry and a pyramidal structure, whereas the BH_3 molecule has D_{3h} symmetry and a planar structure. The planar structure of BH_3 is energetically more favorable than the pyramidal one, by 1.24 eV. Bond strengths were calculated as the total energy difference between the equilibrium structure and the structure with corresponding interatomic distances of 5 Å. For example, the bond strength of NH_3 was defined as the total energy difference between the optimized NH_3 molecule, with the atoms placed 5 Å apart, and then divided by three, that is, the number of N–H bonds. The bond strengths were overestimated, and they were relatively in less agreement with the experiments than the structural properties; this is a typical trend of the LDA calculations. Geometrically, an AB molecule is formed as a combination of NH_3 and BH_3 molecules with C_{3v} symmetry, as shown in Figure 2(a). Bond lengths are 1.024 Å (N–H) and 1.218 Å (B–H), showing no significant difference from those of individual NH_3 and BH_3 molecules. The LAB molecule is formed as a nitrogen-bonded hydrogen atom is replaced by a Li atom, as shown in Figure 2(b). The Li–N bond length is calculated to be 1.845 Å, and one of the B–H bonds near Li is found to be elongated to 1.287 Å (from 1.218 Å). Li substitution reduces the degree of symmetry order (C_{3v}, order 6) of the AB molecule to that of the LAB molecule (C_3, order 3). There are several other possibilities of Li locations, for example, Li substituted with boron-bonded hydrogen, but the total energies in all these cases were found to be much higher than that of the normal LAB system, thus suggesting that they are energetically unfavorable.

We then investigated the crystal structure of AB and LAB by means of DFT calculations. The crystal structure of AB (*c*-AB) has been determined before by neutron diffraction measurements.[28] We used the experimental structural data and performed internal relaxation within DFT: The space group was $Pmn2_1$ (no. 31) and the lattice constants were $a=5.395$ Å, $b=4.887$ Å, and $c=4.986$ Å. The structure of LAB was identified recently by X-ray diffraction (XRD) and supported by DFT.[29] In the same way, we optimized the crystal LAB (*c*-LAB) structure using experimentally determined structural data: The space group was *Pbca* (no. 61) and the lattice constants were $a=7.1051$ Å, $b=13.930$ Å, and $c=5.1477$ Å. The DFT-optimized structural properties of *c*-LAB are listed in Table 3. The number of atoms in an orthorhombic unit cell is 16 for *c*-AB and 64 for *c*-LAB. The molecular and crystal structures of AB and LAB (as a ball-and-stick model) are shown in Figure 2. The detailed structural data of *c*-AB and *c*-LAB, that is, the atomic positions, bond lengths, and intra- and intermolecular distances, were in excellent agreement with previously reported experimental results and theoretical data from the literature, as shown in Tables 2 and 3.

2.2. Electronic Properties

To understand the electronic properties of AB and LAB, we calculated the atomic charges by Hirshfeld analysis,[32] as implemented in the code.[33] The atomic charges were defined relative to the deformation density, that is, relative to the difference between the molecular and unrelaxed atomic charge densities. The calculated atomic charges are listed in Table 4. In a unit molecule of NH_3, the nitrogen atom receives charges from the hydrogen atoms, whereas the boron atom gives charges to the hydrogen atoms in the BH_3 molecule. When they combine, forming an AB molecule, charges from N-bound hydrogen atoms are distributed to other adjacent atoms. This suggests that additional anions would prefer N-bound hydrogen atoms whereas cations would prefer other B atoms, B-bound hydrogen atoms, or N atoms. A similar situation is found in LAB. In a single LAB molecule, B, N, and B-bound hydrogen atoms gain charges from Li and N-bound hydrogen atoms. The tendency is the same for the bulk-crystal cases, but the amount of charge defection from Li in *c*-LAB is reduced to about the half from that in molecular LAB, which

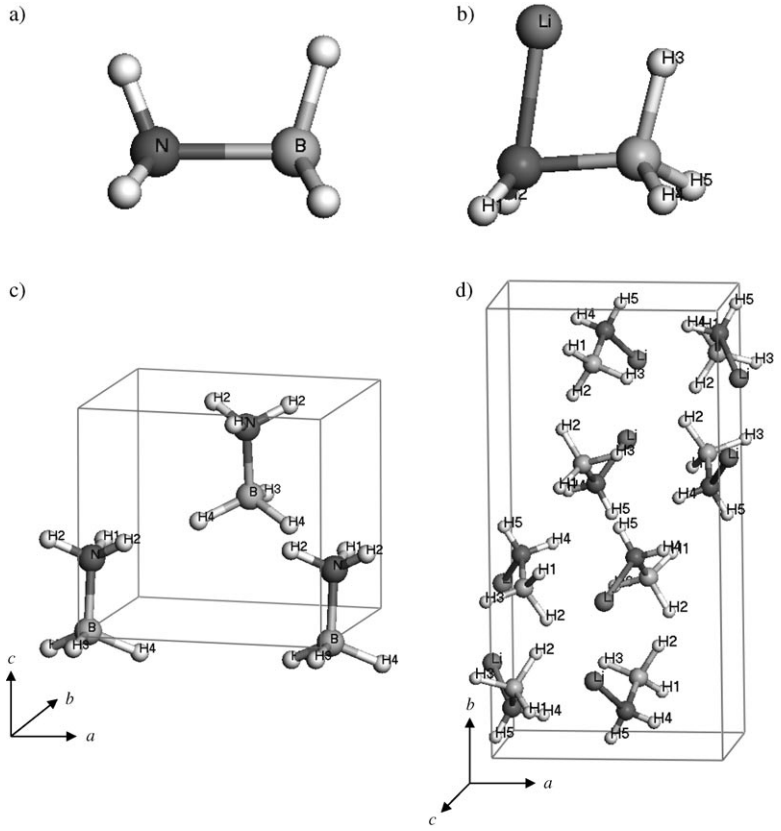

Figure 2. Structures of AB and LAB: a) an AB molecule, b) an LAB molecule, c) an AB crystal [space group: $Pmn2_1$ (No. 31)], and d) an LAB crystal [space group: *Pbca* (No. 61)].

Table 2. Structural properties of *c*-AB.[a–c]

	Theory (present)	Experiment[28]	Theory[29]
	Fractional atomic positions (x, y, z)		
B	(0, 0.1602, −0.0055)	(0, 0.185(3), 0)	–
N	(0, 0.2163, 0.3047)	(0, 0.235(2), 0.314(4))	–
H(1)	(0, 0.4223, 0.3518)	(0, 0.453(7), 0.341(15))	–
H(2)	(0.1556, 0.1299, 0.3950)	(0.140(4), 0.148(5), 0.397(6))	–
H(3)	(0, −0.0908, −0.0376)	(0, −0.043(6), −0.060(6))	–
H(4)	(0.1868, 0.2616, −0.1072)	(0.185(5), 0.264(6), −0.100(5))	–
	Intramolecular distances [Å]		
N–B	1.571	1.58(2)	1.592
N–H	1.042, 1.034	1.07(4), 0.96(3)	1.028, 1.033
B–H	1.233, 1.237	1.15(3), 1.18(3)	1.221, 1.228
	Intermolecular distances [Å]		
H1···H4	2.298	2.21(4)	–
H2···H3	1.897	2.02(3)	–
H2···H4	2.094	2.23(4)	–

[a] The space group is $Pmn2_1$ (No. 31) and the experimental lattice constants are used ($a=5.395$ Å, $b=4.887$ Å, $c=4.986$ Å). [b] The numbers with uncertainty in the experimental column are given in parentheses, as displayed in the original paper.[28] [c] The "–" sign indicates that no relevant data are available.

Table 3. Structural properties of *c*-LAB.[a,b]

	Theory (present)	Experiment[28]	Theory[29]
	Fractional atomic positions (x, y, z)		
B	(0.0945, 0.1540, 0.9658)	(0.091, 0.152, 0.972(5))	(0.09080, 0.14998, 0.96163)
N	(0.0624, 0.0950, 0.7171)	(0.074(1) 0.093(3), 0.716(5))	(0.05593, 0.09003, 0.71334)
H(1)	(0.1783, 0.1115, 0.1473)	(0.149, 0.101, 0.155)	(0.17223, 0.10732, 0.14269)
H(2)	(0.1868, 0.2273, 0.9150)	(0.204, 0.220, 0.945)	(0.18394, 0.22233, 0.90818)
H(3)	(−0.0609, 0.1804, 0.0541)	(−0.064, 0.186, 0.038)	(0.93720, 0.17870, 0.04822)
H(4)	(0.1900, 0.0744, 0.6397)	(0.200, 0.064, 0.661)	(0.18118, 0.06777, 0.63478)
H(5)	(−0.0076, 0.0315, 0.7522)	(−0.018, 0.037, 0.736)	(0.98416, 0.02771, 0.75213)
Li	(−0.0477, 0.1771, 0.4366)	(−0.020(1), 0.180(2), 0.428(3))	(0.93217, 0.17465, 0.43217)
	Intramolecular distances [Å]		
N-B	1.538	1.561(7)	1.547
N-H	1.031	1.025	1.025, 1.026
B-H	1.241, 1.250, 1.256	1.249	1.236, 1.244, 1.248
N-Li	2.002	2.032	2.063
	Intermolecular distances [Å]		
Li···B	2.564, 2.610, 2.646	–	2.50, 2.063, 2.69

[a] The space group is *Pbca* (No. 61) and the experimental lattice constants are used ($a=7.1051$ Å, $b=13.930$ Å, $c=5.1477$ Å). [b] The numbers with uncertainty in the experimental column are given in parentheses, as displayed in the original paper.[29]

Table 4. Atomic charges calculated by the Hirshfeld method[32] (in electron units).[a–c]

Structure	N	B	H (N-bonded)	H (B-bonded)	Li
NH_3	−0.303	–	0.101	–	–
BH_3	–	0.134	–	−0.044	–
AB	−0.054	−0.122	0.164	−0.106	–
LAB	−0.280	−0.129	0.110	−0.103(H3), −0.089 (H4,H5)	0.468
c-AB	−0.066	−0.074	0.131(H1), 0.113(H2)	−0.066(H3), −0.076(H4)	–
c-LAB	−0.233	−0.043	0.101(H4), 0.098(H5)	−0.056(H1), −0.039(H2), −0.047(H3)	0.220

[a] The numbers with a minus sign indicate a gain of charge whereas those with a plus sign indicate a loss of charge. [b] Hydrogen notations can be found in Figure 2. [c] The "–" sign indicates that no relevant data are available.

seems to originate from intermolecular interactions. Such intermolecular interactions significantly affect the physical properties (we will discuss this again in the Vibrational Mode Section).

The volumetric isosurface for the total charge density of *c*-AB is represented by blue dots in Figure 3a. Based on the results of the charge density and the atomic charge analysis, we can assume that the bonds consisting of AB molecules are fairly covalent. To investigate the reactivity, we calculated the Fukui function. Originated from the frontier orbital theory by Fukui[34] and later developed by Yang and Parr,[35] the Fukui

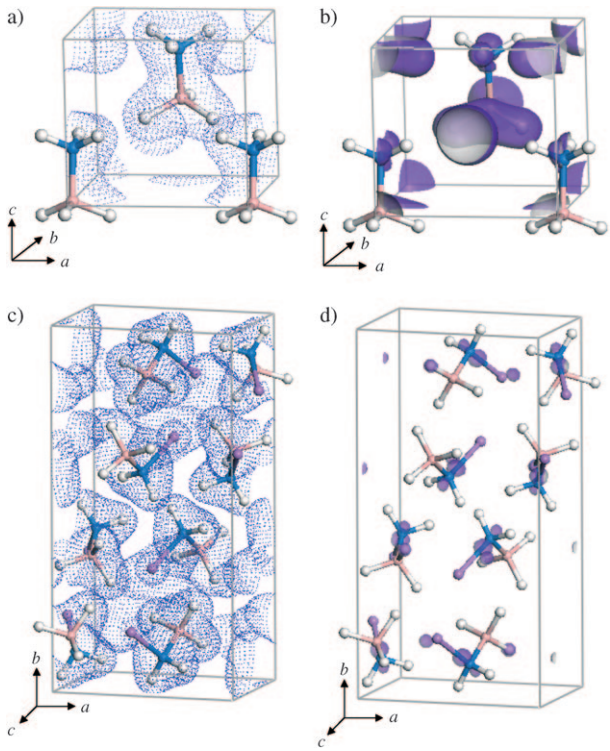

Figure 3. Volumetric isosurfaces of total charge density and Fukui function. a) Total-charge-density plot and b) Fukui function $F^{(-)}$ of *c*-AB. c) Total-charge-density plot and d) Fukui function $F^{(-)}$ of *c*-LAB. The isovalues used were 0.2 e Å^{-3} for the charge density and 0.02 e Å^{-3} for the Fukui function.

function qualitatively measures the sensitivity of the charge density with respect to the loss or gain of electrons. Using the finite difference approximation of the self-consistent charge density of a neutral molecule and that of a cation, the Fukui function $F^{(-)}$ gives the reactivity with respect to the electrophilic attack (i.e. the loss of an electron). The sensitivity to the nucleophilic attack (i.e. the gain of an electron) can be estimated by calculating the Fukui function $F^{(+)}$ using the finite difference approximation of self-consistent charge density of neutral molecules—and that of anions as well. Figure 3b shows the Fukui function $F^{(-)}$ of *c*-AB, that is, the reactivity with respect to an electrophilic attack, with a purple colored isosurface. One can see that the B-bound hydrogen atoms are the most sensitive sites for the electrophilic attack, and the N atom as well, as shown in Figure 3b. The total charge density isosurface of *c*-LAB and the Fukui function $F^{(-)}$ of *c*-LAB are shown in Figures 3c and 3d, respectively. With the same isovalue for the Fukui function $F^{(-)}$ to that of *c*-AB, the reactive site for the electrophilic attack was found to be at the N atom and one of the B-bound hydrogen (H1) atoms. The Fukui function $F^{(-)}$ analysis gives results that are consistent with the atomic-charge data discussed above.

Both the highest occupied molecular orbital (HOMO) and the lowest unoccupied molecular orbital (LUMO) play important roles in the chemical properties of the molecules. We plotted the HOMO and the LUMO of AB and LAB in Figure 4. Precisely speaking, we depicted the square of the eigenwavefunction according to the HOMO or the LUMO, since the wavefunction itself cannot be drawn due to the imaginary part. Cyan- and yellow-colored orbitals represent the plus and minus signs, respectively, in the imaginary term of the eigenwavefunction. In a single AB molecule, the HOMO is around the B atom and the LUMO is around the N-bound hydrogen atoms, as shown in Figure 4a. Figure 4b shows the molecular orbitals of *c*-AB corresponding to the HOMO (i.e. the valence band maximum) and the LUMO (i.e. the conduction band minimum) at the Γ-point. The HOMO is primarily located around boron atoms, similar to the single-molecule case. The LUMO of a molecule is expanded in the bulk system, thereby forming a band-like-shaped orbital (see lower part of Figure 4b). Figure 4c shows the HOMO (upper) and LUMO (lower) of a single LAB molecule. The LUMO of a single LAB molecule is localized at the Li atom, but this feature cannot be found for *c*-LAB, as shown in the right column of Figure 4d.

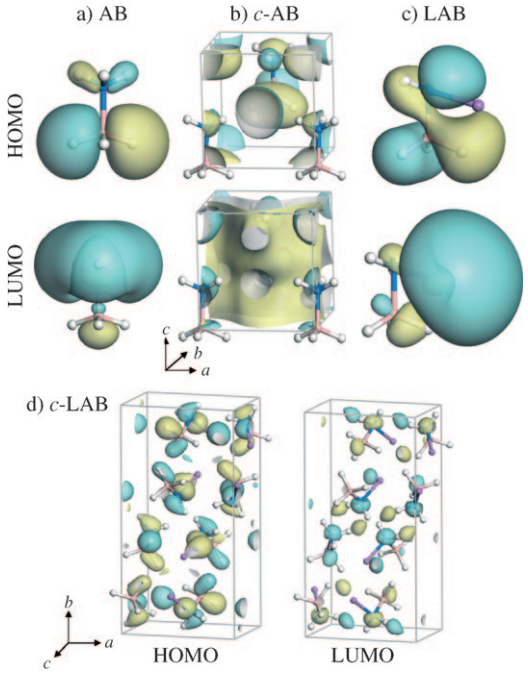

Figure 4. HOMO and LUMO of: a) an AB molecule, b) *c*-AB, c) an LAB molecule, and d) *c*-LAB. An isovalue of 0.03 e Å^{-3} was used.

We investigated the energy levels of several molecules. The HOMO–LUMO gaps of a single molecule were calculated as 3.994 eV (NH_3), 5.363 eV (BH_3), 4.923 eV (AB), and 4.672 eV (LAB), as depicted in Figure 5a. The calculated energy band gap of *c*-AB was 5.850 eV, and the top of the valence band and bottom of the conduction band were at the Γ-point, which indicates a direct band gap. In the case of *c*-LAB, the band gap was 3.945 eV and the valence-band maximum was at the Z-point, that is, (0, 0, 0.5) of the *k*-point, whereas the conduction-band minimum was at the Γ-point, thus indicating an indirect band gap. The band structures are shown in Figures 5b and 5c. However, one should note that the HOMO–LUMO gap or band gap is not well described by conventional DFT calculations using LDA or GGA functionals. More sophisticated calculations, such as the GW approximation, or the use of hybrid functionals are known to overcome this problem.

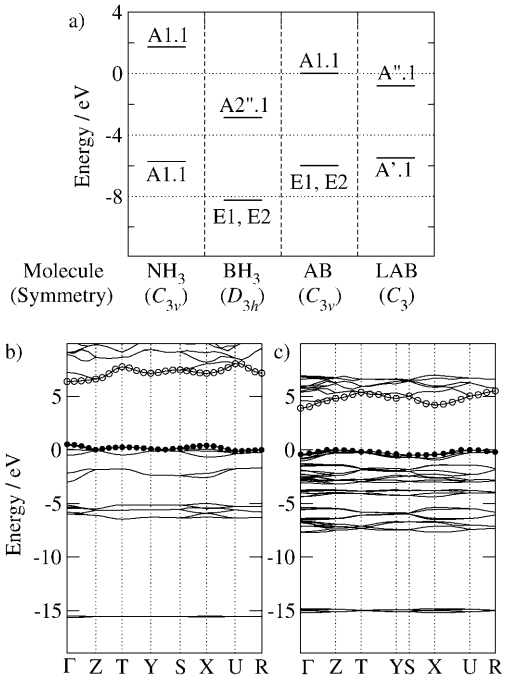

Figure 5. Electronic structures of several molecules, *c*-AB, and *c*-LAB. a) HOMO and LUMO energy-level diagrams of NH_3, BH_3, AB, and LAB molecules. The HOMO levels of BH_3 and AB molecules are doubly degenerated, shown as a thicker line. The band structures of b) *c*-AB and c) *c*-LAB are also shown. The empty circles (○) indicate the LUMO level and the filled ones (●) the HOMO level.

2.3. Vibrational Properties

Vibrational frequencies were computed by diagonalizing the mass-weighted second-derivative Cartesian matrix (i.e. Hessian matrix).[36] The Hessian elements were computed by displacing each atom and computing a gradient vector, thus building up a complete second derivative matrix. In this way, the vibrational modes were calculated numerically. The displacement step size used was 0.01 au (i.e. 0.005 Å) within the harmonic approximation. The Hessian was evaluated using a two-point difference to reduce numerical round-off errors. Intensities were obtained from the atomic polar tensor, which is a second derivative of the total energy with respect to the Cartesian coordinates and dipole moments. The intensity of each mode was evaluated as a square of all the transition moments of the mode and expressed in terms of the atomic polar tensor matrix and eigenvectors of the mass-weighted Hessian. However, mode intensities were unable to be computed in a periodic system with the code we used.

As a benchmark test, we calculated the vibration modes of the NH_3 and BH_3 molecules. The calculated normal modes are listed in Table 5, together with experimental data.[31] The zero-frequency modes (i.e. the rotations and translations) and the intensity-zero modes obtained from the calculations are not listed. In general, the calculated vibrational modes were in good qualitative—and reasonable quantitative—agreement, although they were overestimated by about 2%. This was due to the overestimation of the binding energy, which is a general trend of DFT–LDA calculations, as briefly mentioned in the previous section. From these benchmark tests, we believe that DFT calculations will give reasonable values of the vibrational modes.

The vibration modes of a single AB molecule were calculated. The N–B stretching mode was at 707 cm^{-1}. Normal modes in the low-frequency region (676 and 1002 cm^{-1}) originated from hydrogen wagging modes. The H–B scissors modes (1148 and 1151 cm^{-1}) were lower than the H–N scissors modes (1252 and 1598 cm^{-1}). The stretching mode associated with symmetric (2418 cm^{-1}) and asymmetric (2492 cm^{-1}) motion of the H–B bonds are again lower than symmetric (3398 cm^{-1}) and asymmetric (3519 cm^{-1}) modes from the H–N bonds. Compared to NH_3 and BH_3 molecules, the stretching modes of AB molecule were lowered by about 20 cm^{-1} from the H–N bonds, and by about 150 cm^{-1} from the H–B bonds. The reason why there were more severe changes from the H–B modes was the structural difference between a single BH_3 molecule and the BH_3 part of an AB molecule. BH_3 has a planar structure with 120° as itself, while NH_3 has tetrahedral structure with 106°. Both come to have tetrahedral bonding in the AB structure (see Figure 2a). The number of vibrational modes of an LAB molecule has increased compared to the AB molecule due to the lower geometric symmetry of LAB (C_3, symmetry order 3) compared to AB (C_{3v}, symmetry order 6). The Li-related mode is at 1380 cm^{-1} (Li movement with H–B scissors mode). A strong mode at 1999 cm^{-1} originated from the H–B bond stretching, where the H was located near the Li atom. The N–B stretching mode from LAB was higher (861 cm^{-1}) than that from AB (706 cm^{-1}), which originated from the shorter bond length in LAB (1.644 Å) than AB (1.571 Å). The mode identifications are listed in Table 5, and the simulated spectra of each molecule are depicted as blue lines in Figure 6b.

Table 5. Calculated vibrational modes of several molecules. The frequencies are in cm^{-1}.[a]

Molecule	Theory	Experiment[31]	Vibrational modes
NH_3	1027, 1620	950, 1627	H–N scissors
	3421	3337	H–N symmetric stretching
	3540	3444	H–N antisymmetric stretching
BH_3	1137, 1154	–	H–B scissors
	2504	–	H–B symmetric stretching
	2657	–	H–B antisymmetric stretching
AB	676, 1002	–	H wagging
	706	–	N–B stretching
	1148, 1151	–	H–B scissors
	1252, 1598	–	H–N scissors
	2418	–	H–B symmetric stretching
	2492	–	H–B antisymmetric stretching
	3398	–	H–N symmetric stretching
	3519	–	H–N antisymmetric stretching
LAB	468, 535, 731, 766, 999,1045	–	H wagging
	645	–	Li–N stretching
	861	–	N–B stretching
	1098,1102,1380	–	H–B scissors
	1550	–	H–N scissors
	1999	–	H(3)–B stretching (see Figure 2a)
	2397	–	H–B symmetric stretching
	2450	–	H–B antisymmetric stretching
	3452	–	H–N symmetric stretching
	3526	–	H–N antisymmetric stretching

[a] The "–" sign indicates that no relevant data are available.

Since the samples in the experiments were supposed to have a bulk crystal structure, not a single-molecule structure, we systematically calculated the dimer and crystal systems to compare them with the experimental data and observe the intermolecular effects on the simulated vibrational spectra. Two adjacent molecules from the bulk structures were taken for the dimer geometries. Figure 6 shows theoretically simulated vibrational spectra for the bulk crystal, dimer molecules, and single molecules of AB and LAB. Note that significant variations in the vibrational modes occur upon introducing the inter-molecular interaction as shown in Figure 6, especially in LAB case. It was observed that, because of the inter-molecular interactions, the general shapes of spectra in dimer and crystal are changed and all peaks shifted to the lower energy side compared with

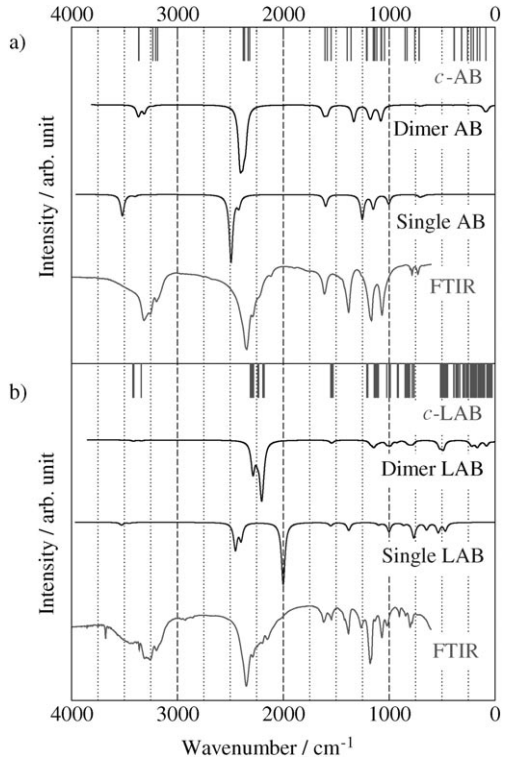

Figure 6. Theoretically simulated (DFT) and experimentally measured (FTIR) vibrational spectra of: a) AB and b) LAB structures: DFT bulk, DFT dimer, DFT single molecule, and FTIR. In the simulated spectra of the molecules we applied a Lorentzian smoothening of 40 cm^{-1} at the full-width-at-half-maximum (FWHM).

that from the single molecule. The *c*-LAB had more atoms per cell as discussed in the previous section while the number of vibration modes thus was more than that of *c*-AB. Modes close each other are shown as a thick line.

We compare theoretically simulated DFT and experimentally measured FTIR vibrational spectra of AB and LAB in Figure 6. We did not expect exact agreement between DFT-simulated and IR-measured spectra, since 1) the simulated ideal system (i.e. no defect, no dopant, and single crystal only) cannot be obtained in realistic experiments, and 2) the symmetry-related selection rule was not considered in our bulk simulations. Nevertheless, we can get physical intuition from simulation and identify the vibrational modes of experimentally observed peaks.

From our DFT simulations, we identified the origin of peaks of *c*-AB as follows: at 726 cm^{-1} as the hydrogen wagging mode [736 ± 20 cm^{-1} (mean value $\pm$standard deviation by DFT calculations)], at 782 cm^{-1} as the N–B stretching mode [839 ± 10 cm^{-1} (DFT)], at 1065 cm^{-1} as the H wagging mode [1065 ± 14 cm^{-1}(DFT)], at 1164 cm^{-1} as the H–B scissors mode [1160 ± 37 cm^{-1} (DFT)], at 1381 cm^{-1} [1377 ± 19 cm^{-1} (DFT)], and 1610 cm^{-1} [1570 ± 24 cm^{-1} (DFT)] as the H–N scissors modes, at 2287 cm^{-1} as the H–B symmetric stretching mode [2324 ± 4 cm^{-1}(DFT)], at 2343 cm^{-1} as the H–B antisymmetric stretching mode [2371 ± 23 cm^{-1}(DFT)], at 3195 cm^{-1} [3193 ± 9 cm^{-1}(DFT)], and 3253 cm^{-1} [3230 cm^{-1}(DFT)] as the H–N symmetric stretching modes, and at 3314 cm^{-1} as the H–N antisymmetric stretching mode [3364 ± 2 cm^{-1}(DFT)]. Deviations for stretching modes were much smaller than those from wagging modes, since the stretching modes were simpler and easier to be described by theoretical calculations than the bending modes.

In the same way, we could identify the peaks of the FTIR spectrum of *c*-LAB as follows: at 800 cm^{-1} [795 ± 20 cm^{-1} (DFT)] and 842 cm^{-1} [838 ± 8 cm^{-1} (DFT)] as H wagging modes, at 901 cm^{-1} as the N–B stretching mode [917 ± 2 cm^{-1} (DFT)], at 1016 cm^{-1} [1001 ± 11 cm^{-1} (DFT)] and 1066 cm^{-1} [1107 ± 7 cm^{-1}(DFT)] as H wagging modes, at 1177 cm^{-1} [1145 ± 29 cm^{-1} (DFT)] and 1261 cm^{-1} [1205 ± 4 cm^{-1} (DFT)] as H–B scissors modes, at 1543 cm^{-1} as the H–N scissors mode [1541 ± 6 cm^{-1} (DFT)], at 2196 cm^{-1} as the H–B symmetric stretching mode [2183 ± 3 cm^{-1}(DFT)], at 2287 cm^{-1} [2249 ± 25 cm^{-1}(DFT)] and 2349 cm^{-1} [2304 ± 20 cm^{-1}(DFT)] as H–B antisymmetric stretching modes, at 3253 cm^{-1} as the H–N symmetric stretching mode [3339 ± 2 cm^{-1}(DFT)], and at 3359 cm^{-1} as the H–N antisymmetric stretching mode [3414 ± 1 cm^{-1}(DFT)]. Vibrational modes and their identifications are summarized in Table 6. Some FTIR peaks could not be identified using our DFT calculations, which could be due to some unknown impurities, such as oxygen or moisture, especially peak at 3675 cm^{-1}. The origin of this peak could be an amine group, alcohols (–OH) or an –NH group.[31] Other possible origins could be the disordered orientations of the NH_3 or BH_3 groups in the experimental sample used in FTIR measurements, or the effect of peak-splitting due to the crystal field. Overall, we could say that we achieved good agreement between theory and experiments for *c*-AB structure, and reasonable agreement for *c*-LAB. Note that the simulated spectra obtained for single molecules were quite different to the other spectra, that is, to the experimental FTIR data and the simulated spectra for the dimer or *c*-LAB (as shown in Figure 6). This suggests that the intermolecular interactions significantly affect the vibrational mode, and they should be considered to achieve a reasonable agreement with the experiments.

3. Conclusions

We have systematically investigated the molecular and bulk crystal forms ammonia borane (NH_3BH_3, AB) and lithium amidoborane ($LiNH_2BH_3$, LAB) by using density functional theory (DFT) calculations. The calculated structural properties were carefully compared to each other and also to the unit molecules of NH_3 and BH_3, and they were in excellent agreement with experimental data. Atomic charge analysis, Fukui functions, and band-gap calculations were shown to analyze the electronic properties of molecular and crystal structures. Electronic structure calculations gave insight into the physical properties of the AB and LAB materials. The vibrational properties were systematically studied by DFT calculations combined with experimental Fourier-transform infrared (FTIR) spectroscopy measurements. We found that the calculated vibration modes of the single molecules were very different from those

Table 6. Calculated vibrational modes of several molecules. The vibrational modes of *c*-AB and *c*-LAB were obtained by means of DFT calculations and FTIR measurements (all the frequencies are given in cm^{-1}).[a]

Structure	Theory	Experiment	Vibrational modes
c-AB	83–317	–	intermolecular stretching
	258	–	H–N rocking
	381, 385	–	H–N, H–B antisymmetric rocking
	715–756	726	H wagging
	829, 848	782	B–N stretching
	1041–1076	1065	H wagging
	1114–1211	1164	H–B scissors
	1358–1603	1381, 1610	H–N scissors
	–	2117	–
	2317, 2330	2287	H–B symmetric stretching
	2364–2377	2343	H–B antisymmetric stretching
	3184–3230	3195, 3253	H–N symmetric stretching
	3362, 3365	3314	H–N antisymmetric stretching
c-LAB	28–331	–	intermolecular stretching
	345–388	–	H–B rocking
	446–469	–	H–N rocking
	478–512	–	H antisymmetric rocking with Li–N stretching
	762–846	800, 842	H wagging
	913–920	901	B–N stretching
	987–1117	1016, 1066	H wagging
	1124–1211	1177, 1261	H–B scissors
	–	1381	–
	1534–1551	1543	H–N scissors
	–	1616	–
	–	2148	–
	2178–2186	2196	H–B symmetric stretching
	2225–2309	2287, 2349	H–B antisymmetric stretching
	–	3197	–
	3335–3342	3253	H–N symmetric stretching
	3412–3415	3359	H–N antisymmetric stretching
	–	3675	–

[a] The "–" sign indicates that no relevant data are available.

of the bulk crystal. The intermolecular interactions significantly affected the vibrational modes and had to be essentially considered to achieve a reasonable comparison with the experimental data. The origin of the peaks in the experimental spectra was successfully identified using the DFT calculation data.

Experimental and Computational Methods

We performed quantum mechanical calculations for AB and LAB molecules and bulk crystals within the DFT framework using a local density approximation (LDA) scheme. The exchange–correlation functional by Predew and Wang[37] was used as implemented in the DMOL3 code.[33] All electron Kohn–Sham wave functions were expanded in a local atomic basis set with each basis function defined numerically on an atomic-centered spherical–polar mesh with a cut-off of 4.4 Å. The double numeric polarized (DNP) basis set was used for all elemental atoms. The DNP basis set corresponds to a double-zeta quality basis set with a *p*-type polarization function added to hydrogen and *d*-type polarization functions added to other atoms. Geometries were optimized until the maximum force on each atom was less than 0.002 Ha $Å^{-1}$, the maximum displacement was less than 0.005 Å, and the total energy change was less than 10^{-5} Ha. The energy tolerance in self-consistent field calculations was 10^{-6} Ha. Monkhorst-Pack's ***k***-point scheme[38] was used with a spacing of ca. 0.04 $Å^{-1}$ [i.e. (5×5×5) for *c*-AB, (4×2×5) for *c*-LAB] to sample the Brillouin-zone.

The AB sample was synthesized by the chemical reaction of $(NH_4)_2CO_3/NaBH_4$ in tetrahydrofuran (THF). The LAB sample was prepared by means of two-hour mechanical ball-milling of the AB/LiH mixture. A detailed description of the sample preparation can be found in our previous paper.[26] FTIR spectra were recorded at room temperature on a Bruker TENSOR 27 spectrometer using KBr pellets. The samples were prepared in an Ar-filled glove box by grinding a small amount of the samples with dry spectroscopic-grade KBr in an agate mortar and pestle and pressed into a pellet for analysis. Each spectrum was acquired after 64 scans with a resolution of 4 cm^{-1}.

Acknowledgements

This research at KRISS was performed for the Hydrogen Energy R&D Center, one of the 21st Century Frontier R&D Programs, funded by the Ministry of Education, Science and Technology of Korea. The work at Shenyang National Laboratory for Materials Science was financially supported by the Hundred Talents Project of Chinese Academy of Sciences (CAS), NSFC (Nos. 50771094 and 50801059), the Frontier Project of CAS Knowledge Innovation Program (No. KGCXZ-YW-342) and the species funding for CAS President Prize winner. The work at SKKU was supported by the MOE through the STAR-faculty project and TND project, WCU program through the Korea Science and Engineering Foundation funded by the Ministry of Education, Science and Technology (R31-2008-000-10029-0), and KOSEF through CNNC at SKKU.

Keywords: density functional calculations · electronic structure · FTIR spectroscopy · hydrogen storage · vibrational spectroscopy

[1] R. C. Bowman, Jr., B. Fultz, *MRS Bull.* **2002**, *27*, 688–693.
[2] A. C. Dillon, K. M. Jones, T. A. Bekkedahl, C. H. Kiang, D. S. Bethune, M. J. Heben, *Nature* **1997**, *386*, 377–379.
[3] P. Chen, X. Wu, J. Lin, K. L. Tan, *Science* **1999**, *285*, 91–93.
[4] Y. Ye, C. C. Ahn, C. Witham, B. Fultz, J. Liu, A. G. Rinzler, D. Colbert, K. A. Smith, R. E. Smalley, *Appl. Phys. Lett.* **1999**, *74*, 2307–2309.
[5] Y. Y. Fan, B. Liao, M. Liu, Y. L. Wie, M. Q. Lu, H. M. Cheng, *Carbon* **1999**, *37*, 1649–1652.

[6] a) S. M. Lee, Y. H. Lee, *Appl. Phys. Lett.* **2000**, *76*, 2877–2879; b) S. M. Lee, Y. H. Lee, *Appl. Phys. Lett.* **2002**, *81*, 184.
[7] S. M. Lee, K. H. An, Y. H. Lee, G. Seifert, Th. Frauenheim, *J. Am. Chem. Soc.* **2001**, *123*, 5059–5063.
[8] V. Meregalli, M. Parrinello, *Appl. Phys. A* **2001**, *72*, 143–146.
[9] B. K. Gupta, O. N. Srivastava, *Int. J. Hydrogen Energy* **2001**, *26*, 857–862.
[10] M. Hirscher, M. Becher, M. Haluska, U. Dettlaff-Weglikowska, Q. Quintel, G. S. Duesberg, Y.-M. Choi, P. Downes, M. Hulmas, S. Roth, I. Stepanek, P. Bernier, *Appl. Phys. A* **2001**, *72*, 129–132.
[11] S. C. Lim, K. K. Kim, S. H. Jeong, K. H. An, S. B. Lee, Y. H. Lee, *Int. J. Hydrogen Energy* **2007**, *32*, 3442–3447.
[12] S. A. Shevlin, Z. X. Guo, *Chem. Soc. Rev.* **2009**, *38*, 211–225.
[13] R. T. Yang, *Carbon* **2000**, *38*, 623–626.
[14] F. E. Pinkerton, B. G. Wicke, C. H. Olk, G. G. Tibbetts, G. P. Meisner, M. S. Meyer, J. F. Herbst, *J. Phys. Chem. B* **2000**, *104*, 9460–9467.
[15] L. Schlapbach, A. Züttel, *Nature* **2001**, *414*, 353–358.
[16] Hydrogen, Fuel Cells & Infrastructure Technologies program: Multi-Year Research, development and Demonstration Plan, Technical Plan, Hydrogen storage, **2007**, http://www1.eere.energy.gov/hydrogenandfuelcells/mypp.
[17] M. Becher, M. Haluska, M. Hirscher, A. Quintel, V. Skakalova, U. Dettlaff-Weglikovska, U. X. Chen, M. Hulman, Y. Choi, S. Roth, V. Meregalli, M. Parrinello, R. Ströbel, L. Jörissen, M. M. Kappers, J. Fink, A. Züttel, I. Stepanek, P. Bernier, *Physique* **2003**, *4*, 1055–1062.
[18] A. N. Kolmogorov, R. Drautz, D. G. Pettifor, *Phys. Rev. B* **2007**, *76*, 184102.
[19] H. Lee, W. I. Choi, J. Ihm, *Phys. Rev. Lett.* **2006**, *97*, 056104.
[20] Y.-H. Kim, Y. Zhao, A. Williamson, M. J. Heben, S. B. Zhang, *Phys. Rev. Lett.* **2006**, *96*, 106 102.
[21] A. G. Wong-Foy, A. J. Matzger, O. M. Yaghi, *J. Am. Chem. Soc.* **2006**, *128*, 3494–3495.
[22] S. S. Han, H. Furukawa, O. M. Yaghi, W. A. Goddard III, *J. Am. Chem. Soc.* **2008**, *130*, 11580–11581.
[23] F. Stephens, V. Pons, R. T. Baker, *Dalton Trans.* **2007**, 2613.
[24] J. Baumann, F. Baitalow, G. Wolf, *Thermochim. Acta* **2005**, *430*, 9–14.
[25] G. W. Crabtree, M. S. Dresselhaus, *MRS Bull.* **2008**, *32*, 421–428.
[26] X. Kang, Z. Fang, L. Kong, H. Cheng, X. Yao, G. Lu, P. Wang, *Adv. Mater.* **2008**, *20*, 2756–2759.
[27] T. B. Richardson, S. de Gala, R. H. Crabtree, P. E. M. Siegbahn, *J. Am. Chem. Soc.* **1995**, *117*, 12875–12876.
[28] W. T. Klooster, T. F. Koetzle, P. E. M. Siegbahn, T. B. Richardson, R. H. Crabtree, *J. Am. Chem. Soc.* **1999**, *121*, 6337–6343.
[29] H. Wu, W. Zhou, T. Yildirim, *J. Am. Chem. Soc.* **2008**, *130*, 14834–14839.
[30] Z. Xiong, C. K. Yong, G. Wu, P. Chen, W. Shaw, A. Karkamkar, T. Autrey, M. O. Jones, S. R. Johnson, P. P. Edwards, W. I. F. David, *Nat. Mater.* **2008**, *7*, 138–141.
[31] *Handbook of Chemistry and Physics, 84th ed.*, CRC, Boca Raton, **2003–2004**.
[32] F. L. Hirshfeld, *Theor. Chim. Acta B* **1977**, *44*, 129–138.
[33] a) B. Delley, *J. Chem. Phys.* **1990**, *92*, 508–517; b) B. Delley, *J. Chem. Phys.* **2000**, *113*, 7756–7764.
[34] K. Fukui, *Science* **1982**, *218*, 747–754.
[35] R. G. Parr, W. Yang, *Density-functional Theory of Atoms and Molecules*, Oxford University Press, New York, **1989**.
[36] E. B. Wilson, J. C. Decius, P. C. Cross, *Molecular Vibrations*, Dover, New York, **1980**.
[37] J. P. Perdew, Y. Wang, *Phys. Rev. B* **1992**, *45*, 13244–13249.
[38] a) J. D. Pack, H. Monkhorst, *Phys. Rev. B* **1976**, *13*, 5188–5192; b) J. D. Pack, H. Monkhorst, *Phys. Rev. B* **1977**, *16*, 1748–1749.

Received: April 10, 2009
Published online on July 13, 2009

